Biomedical Optics EXPRESS

28 MHz swept source at 1.0 μm for ultrafast quantitative phase imaging

Xiaoming Wei, Andy K. S. Lau, Yiqing Xu, Kevin K. Tsia, and Kenneth K. Y. Wong*

Department of Electrical and Electronic Engineering, The University of Hong Kong, Pokfulam Road, Hong Kong, China

*kywong@eee.hku.hk

Abstract: Emerging high-throughput optical imaging modalities, in particular those providing phase information, necessitate a demanding speed regime (e.g. megahertz sweep rate) for those conventional swept sources; while an effective solution is yet to be demonstrated. We demonstrate a stable breathing laser as inertia-free swept source (BLISS) operating at a wavelength sweep rate of 28 MHz, particularly for the ultrafast interferometric imaging modality at 1.0 μm. Leveraging a tunable dispersion compensation element inside the laser cavity, the wavelength sweep range of BLISS can be tuned from ~10 nm to ~63 nm. It exhibits a good intensity stability, which is quantified by the ratio of standard deviation to the mean of the pulse intensity, i.e. 1.6%. Its excellent wavelength repeatability, <0.05% per sweep, enables the single-shot imaging at an ultrafast line-scan rate without averaging. To showcase its potential applications, it is applied to the ultrafast (28-MHz line-scan rate) interferometric time-stretch (iTS) microscope to provide quantitative morphological information on a biological specimen at a lateral resolution of 1.2 μm. This fiber-based inertia-free swept source is demonstrated to be robust and broadband, and can be applied to other established imaging modalities, such as optical coherence tomography (OCT), of which an axial resolution better than 12 μm can be achieved.

OCIS codes: (140.4050) Mode-locked lasers; (140.3615) Lasers, ytterbium; (110.3175) Interferometric imaging.

References and links

1. S. H. Yun, D. J. Richardson, and B. Y. Kim, "Interrogation of fiber grating sensor arrays with a wavelength-swept fiber laser," Opt. Lett. **23**(11), 843–845 (1998).
2. K. J. Gasvik, Optical Metrology, (3rd Ed. John Wiley and Sons, Sussex 2003).
3. N. V. Tkachenko, Optical spectroscopy: methods and instrumentations, (Elsevier, Oxford, UK, 2006).
4. D. Huang, E. A. Swanson, C. P. Lin, J. S. Schuman, W. G. Stinson, W. Chang, M. R. Hee, T. Flotte, K. Gregory, C. A. Puliafito, and J. G. Fujimoto, "Optical coherence tomography," Science **254**(5035), 1178–1181 (1991).
5. G. J. Tearney, R. H. Webb, and B. E. Bouma, "Spectrally encoded confocal microscopy," Opt. Lett. **23**(15), 1152–1154 (1998).
6. S. Bégin, B. Burgoyne, V. Mercier, A. Villeneuve, R. Vallée, and D. Côté, "Coherent anti-Stokes Raman scattering hyperspectral tissue imaging with a wavelength-swept system," Biomed. Opt. Express **2**(5), 1296–1306 (2011).
7. S. H. Yun, C. Boudoux, G. J. Tearney, and B. E. Bouma, "High-speed wavelength-swept semiconductor laser with a polygon-scanner-based wavelength filter," Opt. Lett. **28**(20), 1981–1983 (2003).
8. R. Huber, M. Wojtkowski, and J. G. Fujimoto, "Fourier Domain Mode Locking (FDML): A new laser operating regime and applications for optical coherence tomography," Opt. Express **14**(8), 3225–3237 (2006).
9. Y. Takubo and S. Yamashita, "High-speed dispersion-tuned wavelength-swept fiber laser using a reflective SOA and a chirped FBG," Opt. Express **21**(4), 5130–5139 (2013).
10. M. Bonesi, M. P. Minneman, J. Ensher, B. Zabihian, H. Sattmann, P. Boschert, E. Hoover, R. A. Leitgeb, M. Crawford, and W. Drexler, "Akinetic all-semiconductor programmable swept-source at 1550 nm and 1310 nm with centimeters coherence length," Opt. Express **22**(3), 2632–2655 (2014).
11. W. Wieser, B. R. Biedermann, T. Klein, C. M. Eigenwillig, and R. Huber, "Multi-Megahertz OCT: High quality 3D imaging at 20 million A-scans and 4.5 GVoxels per second," Opt. Express **18**(14), 14685–14704 (2010).
12. T. Klein, W. Wieser, L. Reznicek, A. Neubauer, A. Kampik, and R. Huber, "Multi-MHz retinal OCT," Biomed. Opt. Express **4**(10), 1890–1908 (2013).

#245496 Received 6 Jul 2015; revised 18 Aug 2015; accepted 31 Aug 2015; published 8 Sep 2015

13. B. Potsaid, V. Jayaraman, J. G. Fujimoto, J. Jiang, P. J. S. Heim, and A. E. Cable, "MEMS tunable VCSEL light source for ultrahigh speed 60kHz-1MHz axial scan rate and long range centimeter class OCT imaging," in SPIE BiOS, (International Society for Optics and Photonics, 2012), 82130M–82130M–82138.
14. I. Grulkowski, J. J. Liu, B. Potsaid, V. Jayaraman, C. D. Lu, J. Jiang, A. E. Cable, J. S. Duker, and J. G. Fujimoto, "Retinal, anterior segment and full eye imaging using ultrahigh speed swept source OCT with vertical-cavity surface emitting lasers," Biomed. Opt. Express **3**(11), 2733–2751 (2012).
15. K. Goda, K. K. Tsia, and B. Jalali, "Serial time-encoded amplified imaging for real-time observation of fast dynamic phenomena," Nature **458**(7242), 1145–1149 (2009).
16. R. E. Saperstein, N. Alic, S. Zamek, K. Ikeda, B. Slutsky, and Y. Fainman, "Processing advantages of linear chirped fiber Bragg gratings in the time domain realization of optical frequency-domain reflectometry," Opt. Express **15**(23), 15464–15479 (2007).
17. D. R. Solli, J. Chou, and B. Jalali, "Amplified wavelength–time transformation for real-time spectroscopy," Nat. Photonics **2**(1), 48–51 (2008).
18. S. Moon and D. Y. Kim, "Ultra-high-speed optical coherence tomography with a stretched pulse supercontinuum source," Opt. Express **14**(24), 11575–11584 (2006).
19. K. Goda, A. Fard, O. Malik, G. Fu, A. Quach, and B. Jalali, "High-throughput optical coherence tomography at 800 nm," Opt. Express **20**(18), 19612–19617 (2012).
20. J. Xu, C. Zhang, J. Xu, K. K. Y. Wong, and K. K. Tsia, "Megahertz all-optical swept-source optical coherence tomography based on broadband amplified optical time-stretch," Opt. Lett. **39**(3), 622–625 (2014).
21. J. Xu, X. Wei, L. Yu, C. Zhang, J. Xu, K. K. Y. Wong, and K. K. Tsia, "Performance of megahertz amplified optical time-stretch optical coherence tomography (AOT-OCT)," Opt. Express **22**(19), 22498–22512 (2014).
22. T. Huo, C. Wang, X. Zhang, T. Chen, W. Liao, W. Zhang, S. Ai, J. C. Hsieh, and P. Xue, "Ultrahigh-speed optical coherence tomography utilizing all-optical 40 MHz swept-source," J. Biomed. Opt. **20**(3), 030503 (2015).
23. K. Goda, A. Mahjoubfar, C. Wang, A. Fard, J. Adam, D. R. Gossett, A. Ayazi, E. Sollier, O. Malik, E. Chen, Y. Liu, R. Brown, N. Sarkhosh, D. Di Carlo, and B. Jalali, "Hybrid Dispersion Laser Scanner," Sci. Rep. **2**, 445 (2012).
24. A. Yazaki, C. Kim, J. Chan, A. Mahjoubfar, K. Goda, M. Watanabe, and B. Jalali, "Ultrafast dark-field surface inspection with hybrid-dispersion laser scanning," Appl. Phys. Lett. **104**(25), 251106 (2014).
25. S. K. Kalyoncu, R. Torun, Y. Huang, Q. Zhao, and O. Boyraz, "Fast dispersive laser scanner by using digital micro mirror arrays," J. Micro Nano Manuf. **2**(2), 021004 (2014).
26. C. L. Chen, A. Mahjoubfar, and B. Jalali, "Optical data compression in time stretch imaging," PLoS One **10**(4), e0125106 (2015).
27. X. Wei, J. Xu, Y. Xu, L. Yu, J. Xu, B. Li, A. K. S. Lau, X. Wang, C. Zhang, K. K. Tsia, and K. K. Y. Wong, "Breathing laser as an inertia-free swept source for high-quality ultrafast optical bioimaging," Opt. Lett. **39**(23), 6593–6596 (2014).
28. K. Tamura, E. P. Ippen, H. A. Haus, and L. E. Nelson, "77-fs pulse generation from a stretched-pulse mode-locked all-fiber ring laser," Opt. Lett. **18**(13), 1080–1082 (1993).
29. F. Ilday, J. Chen, and F. Kärtner, "Generation of sub-100-fs pulses at up to 200 MHz repetition rate from a passively mode-locked Yb-doped fiber laser," Opt. Express **13**(7), 2716–2721 (2005).
30. X. Wei, Y. Xu, A. K. S. Lau, K. K. Tsia, and K. K. Y. Wong, "Ultrafast swept source at 1.0 μm for high-speed phase sensitive imaging," in Optics in the Life Sciences, OSA Technical Digest (online) (Optical Society of America, 2015), paper BW2A.2.
31. D. J. Richardson, J. Nilsson, and W. A. Clarkson, "High power fiber lasers: current status and future perspectives [Invited]," J. Opt. Soc. Am. B **27**(11), B63–B92 (2010).
32. A. Mahjoubfar, C. Chen, K. R. Niazi, S. Rabizadeh, and B. Jalali, "Label-free high-throughput cell screening in flow," Biomed. Opt. Express **4**(9), 1618–1625 (2013).
33. A. K. S. Lau, T. T. W. Wong, K. K. Y. Ho, M. T. H. Tang, A. C. S. Chan, X. Wei, E. Y. Lam, H. C. Shum, K. K. Y. Wong, and K. K. Tsia, "Interferometric time-stretch microscopy for ultrafast quantitative cellular and tissue imaging at 1 μm," J. Biomed. Opt. **19**(7), 076001 (2014).
34. A. Chong, J. Buckley, W. Renninger, and F. Wise, "All-normal-dispersion femtosecond fiber laser," Opt. Express **14**(21), 10095–10100 (2006).
35. A. Chong, H. Liu, B. Nie, B. G. Bale, S. Wabnitz, W. H. Renninger, M. Dantus, and F. W. Wise, "Pulse generation without gain-bandwidth limitation in a laser with self-similar evolution," Opt. Express **20**(13), 14213–14220 (2012).
36. P. Russell, "Photonic crystal fibers," Science **299**(5605), 358–362 (2003).
37. R. Leitgeb, C. Hitzenberger, and A. Fercher, "Performance of fourier domain vs. time domain optical coherence tomography," Opt. Express **11**(8), 889–894 (2003).
38. K. K. Tsia, K. Goda, D. Capewell, and B. Jalali, "Performance of serial time-encoded amplified microscope," Opt. Express **18**(10), 10016–10028 (2010).
39. G. Popescu, Quantitative Phase Imaging of Cells and Tissues, McGraw Hill, New York, United States (2011).

1. Introduction

Ultrastable swept sources at an ultrafast sweep rate are the "holy grail" for a wide range of spectrally-encoded applications [1–6], especially the phase sensitive imaging. Conventionally, swept sources are implemented with active wavelength scanning

#245496 Received 6 Jul 2015; revised 18 Aug 2015; accepted 31 Aug 2015; published 8 Sep 2015

mechanisms, either mechanical or electrical tuning [7–10]. The sweep rate based on those methods, however, is largely limited to the kHz range, which is order of magnitude slower than the MHz regime required by ultrafast phenomena studies or high-throughput screening applications. Techniques, such as time-multiplexing with buffer stages [11,12] and microelectromechanical systems (MEMS) [13,14], have recently been incorporated to enable MHz wavelength sweeping. A 10's MHz sweep rate, unfortunately, is still a largely unexplored regime and requiring efforts for those active wavelength scanning methods. Optical time-stretch, on the other hand, is a passive wavelength scanning technique without mechanical inertia [15–17]. By leveraging a dispersive element, such as the optical fiber and linearly chirped fiber Bragg grating with large group-velocity dispersion (GVD), it spreads the wavelengths of the pulsed lightwave in the time domain. Although successfully applied in the areas such as time-stretch microscope [15], ultrafast spectroscope [17], and optical coherence tomography (OCT) [18–22], it is largely under-explored as ultrastable swept sources, particularly in terms of sweeping bandwidth and stability. In this regard, recently several works have devoted to the speed improvement of the swept source through optical time-stretch technique, particularly in the wavelength windows of 800 nm [23,24] and 1550 nm [25,26]. We also proposed a stable 11.5-MHz breathing laser as inertia-free swept source (BLISS) and achieved a sweep range of ~60 nm in the 1550-nm window [27], which was benefitted from the dispersion engineering [28,29]. The phase stability, or the wavelength repeatability from sweep to sweep, which is much more stringent for phase sensitive imaging modalities, unfortunately has not been studied in the prior works. On the other hand, it is interesting to investigate the ultrahigh-speed swept source in the 1.0-μm window [30], because of a lower tissue absorption and scattering. Furthermore, by far the most developed fiber gain media in terms of efficiency and gain bandwidth has been devoted to this wavelength window [31], which makes it feasible to generate ultrafast high-power wideband swept source.

In this paper, we demonstrate a bandwidth-tunable BLISS at 1.0 μm with a record product of sweep rate and bandwidth, i.e. 1764 MHz•nm, at 28 MHz and 63 nm, respectively. To perform pulse breathing for broadband operation, we incorporate a tunable dispersion-compensating module (DCM) inside the laser cavity, such that the wavelength sweep range can be tuned from ~10 nm to ~63 nm. Both intensity and phase stabilities of 1.0-μm BLISS are studied with real-time techniques. To showcase its potential utility in the phase-sensitive imaging, we apply it to the emerging interferometric time-stretch (iTS) microscope [32,33]. Single-shot interferometric imaging of biological specimen is obtained with a spatial resolution of 1.2 μm at a frame rate of 28 MHz.

2. Experimental setup

Figure 1 illustrates the experimental setup of the 1.0-μm swept source and iTS microscope. The swept source was constructed with a ring cavity consisted of four parts: 1) amplification, 2) mode-locking, 3) dispersion tuning and 4) wavelength sweeping. 1) A piece of 60-cm ytterbium-doped fiber (YDF, Thorlabs) was served as the gain medium. It was pumped by a 980-nm fiber-pigtailed laser diode through the 980-nm port of a fiber-based wavelength-division multiplexing (WDM) coupler. 2) The mode-locking was performed by additive pulse mode-locking (APM) technique [28], also known as nonlinear polarization rotation (NPR) mode-locking in fiber optics [29]. To achieve polarization-dependent loss for pulse compression, a polarization beam splitter (PBS) with polarization-maintain fiber pigtail was used. One port with 45° alignment to the incident polarization was looped back to the cavity for oscillation, while another port served as the output. Two in-line polarization controllers (PC) were employed to adjust the state of polarization (SOP) of the lightwave inside the cavity. In principle, only one PC is enough for APM, while two can provide a more flexible polarization control. PBS and PCs cooperated to realize the APM operation—PBS can transmit the peak of the incident pulse while block the edge by adjusting the orientation of PCs. With enough round trips, an initial noise pulse can be compressed to a stable ultrashort pulse. A polarization-insensitive isolator (ISO) was utilized to not only ensure the

#245496 Received 6 Jul 2015; revised 18 Aug 2015; accepted 31 Aug 2015; published 8 Sep 2015

unidirectional operation, but also facilitate the self-starting mode-locking. 3) As the glass fiber has a normal dispersion at 1.0 μm, it naturally works in the all-normal dispersion regime for mode-locked fiber lasers, and bandpass filters are usually incorporated to obtain mode-locking [34]. The mode-locked bandwidth, however, would be limited by that of bandpass filters, typically ~10 nm. Although nonlinear propagation in a normal-dispersion cavity can broaden its spectrum further [35], it does not facilitate the phase stability owing to the detrimental nonlinear effect [27]. As a consequence, we introduced the anomalous dispersion to compensate the normal dispersion, which performed pulse breathing and thus stably delivered broadband APM mode-locking [28]. The anomalous dispersion was achieved through a diffraction grating pair with a tunable spacing, i.e. the DCM in Fig. 1, resulting in tunable net dispersion as well as APM spectral width. The total cavity length was ~6.9 m, yielding a repetition rate of ~28.3 MHz. 4) To achieve wavelength sweeping through optical time-stretch, the APM pulse from the cavity was double-passed through a 5-km single-mode fiber (SMF) with a total GVD of –0.36 ns/nm at 1060 nm. The wavelength-swept pulse was finally launched into the iTS imaging system through a circulator (CL), which will be described later.

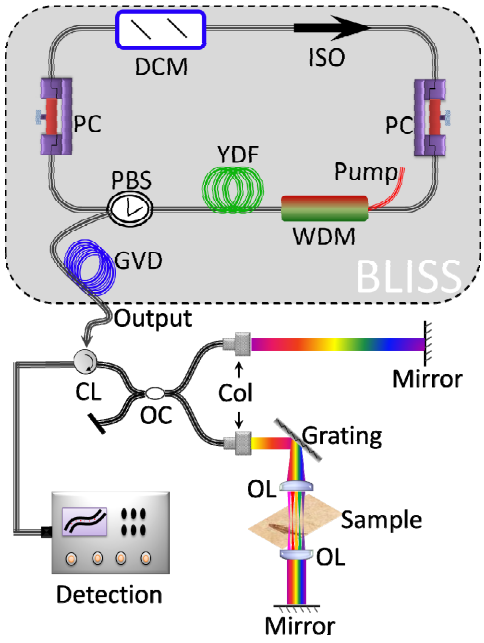

Fig. 1. The experimental setup of the 1.0-μm BLISS and iTS microscope.

3. Results and discussion

The continuous-wave (CW) mode-locked threshold of the 1.0-μm BLISS was ~330 mW. The relatively high threshold is due to an insertion loss of the DCM, i.e. ~6.5 dB. For a higher power efficiency and all-fiber design, grating-based DCM can be replaced by dispersion-engineered fibers, e.g. photonic crystal fiber (PCF) [36]. By tuning the separation of the grating pair from ~10 mm to ~40 mm with an incident angle of ~50°, the net dispersion of the cavity can cover both anomalous and normal dispersion regimes, but close to zero in favor of broadband mode-locking. The net dispersion of the cavity was always set to the slightly-normal dispersion regime, based on the fact that it delivers a rectangle-shaped spectrum with better flatness [34]. As shown in Fig. 2, the optical spectrum of BLISS pulse was gradually broadened as the net dispersion was approaching to zero from the normal dispersion regime. It is noted that, the spectral width of present setup was not limited to 63 nm, while a wider

#245496 Received 6 Jul 2015; revised 18 Aug 2015; accepted 31 Aug 2015; published 8 Sep 2015

mode-locked spectrum exhibited soliton fission and Raman effect, and delivered a poor performance in the time-stretch process owing to the severe phase fluctuation. Considering the bandwidth limitation of the optical amplifications for different applications at 1.0 μm, we set the spectral bandwidth of BLISS to be ~55 nm characterized by the steep edges for the rest of experiments. The corresponding output power was ~25 mW.

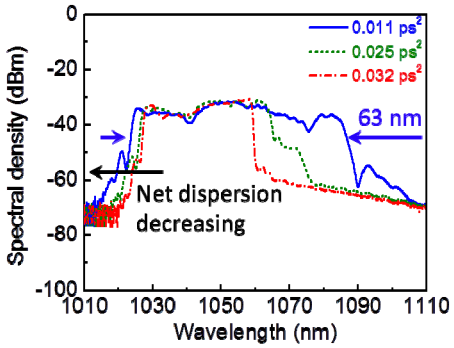

Fig. 2. The spectral tunability of the 1.0-μm BLISS. Noted, the net dispersion of the cavity was tuned by adjusting the separation of the grating pair, resulting in net dispersion amounts of ~0.032 ps^2 (red), ~0.025 ps^2 (green) and ~0.011 ps^2 (blue), respecrively.

The temporal spacing between the neighboring pulses was 35.3 ns (~28.3 MHz), which was detected by a picosecond photodetector with a bandwidth of 8 GHz (Picometrix AD-50xr) and recorded by a 16-GHz real-time oscilloscope (Agilent DSO-X 91604A). Specifically, multiple pulse or even bound-soliton inside the cavity is expected to go against the linear sweep in the time-stretch process. To verify it, we examined the APM pulse simultaneously by the real-time oscilloscope and another autocorrelator (Femtochrome FR-103HS). It was observed that single pulse operation was always guaranteed. A 500-μs-long pulse train, up to the maximum memory depth of the real-time oscilloscope, i.e. 50 Mpt, was recorded at a sampling rate of 80 GSa/s. and can be used to study the intensity stability of the APM pulse. 14,000 consecutive pulses were then utilized to calculate the intensity histogram, as shown in Fig. 3(a), where the red curve is the Gaussian fitting. As can be observed, the stable intensity operation was confirmed by a narrow and Gaussian-like distribution. The ratio of standard deviation to the mean (Std/mean) of the pulse intensity was calculated to be 1.6% over 14,000 pulses. We also measured the std/mean of a commercial mode-locked laser (Time-Bandwidth Lynx) as a reference, and obtained a comparable value, i.e. 1.7%, but giving a much narrower bandwidth, i.e. < 0.5 nm. We further measured its radio frequency (rf) power spectral density (PSD) to examine its relative intensity noise. As shown in Fig. 3(b), where the spectrum has been normalized to decibels relative to the carrier per hertz (dBc/Hz), the shot-noise limit (background noise) for our measurement system is about −120 dBc/Hz, with a 26-GHz rf spectrum analyzer (Agilent E4440A). The PSD of APM pulses did not exhibit an obvious raise of the noise floor, and result in a signal-to-noise ratio (SNR) of ~103 dB at a resolution bandwidth of 10 Hz, which is also verified by intensity histogram shown as the inset of Fig. 3(a).

#245496 Received 6 Jul 2015; revised 18 Aug 2015; accepted 31 Aug 2015; published 8 Sep 2015

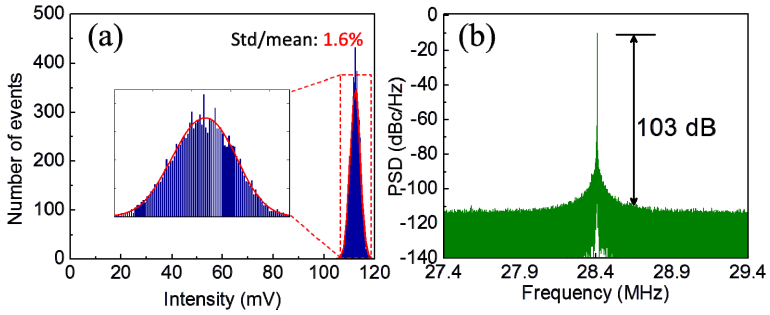

Fig. 3. (a) The intensity histogram of APM pulse train. (b) The rf power spectral density of APM pusle with a rf range of 2 MHz. The resolution bandwidth was set to 10 Hz.

All-optical wavelength sweeping was obtained by passing the APM pulse through the GVD element with a total dispersion of −0.36 ns/nm to perform frequency-to-time mapping. The wavelength-swept waveform was measured by the real-time oscilloscope and shown in Fig. 4. The temporal width of the stretched pulse was ~20 ns, yielding a duty cycle of 56.6%. A 100% duty cycle can be obtained by prolonging the GVD fiber to about 8.8 km, which is unfortunately not available in our laboratory. To further examine stabilities of spectral intensity and width from frame to frame, we recorded 8192 wavelength-swept pulses in real-time and then overlapped them together, as shown in Fig. 4(b). Ignoring the noise background (noise amplitude of ~2 mV) of the detecting system, it exhibits a reasonably good performance in terms of intensity and timing jitter, i.e. the spectral width stability.

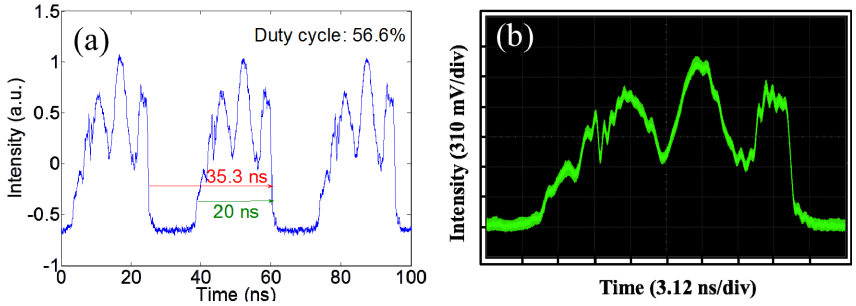

Fig. 4. (a) The wavelength-swept waveform of the 1.0-μm BLISS. (b) 8192 wavelength-swept BLISS pulses overlapped together.

#245496 Received 6 Jul 2015; revised 18 Aug 2015; accepted 31 Aug 2015; published 8 Sep 2015

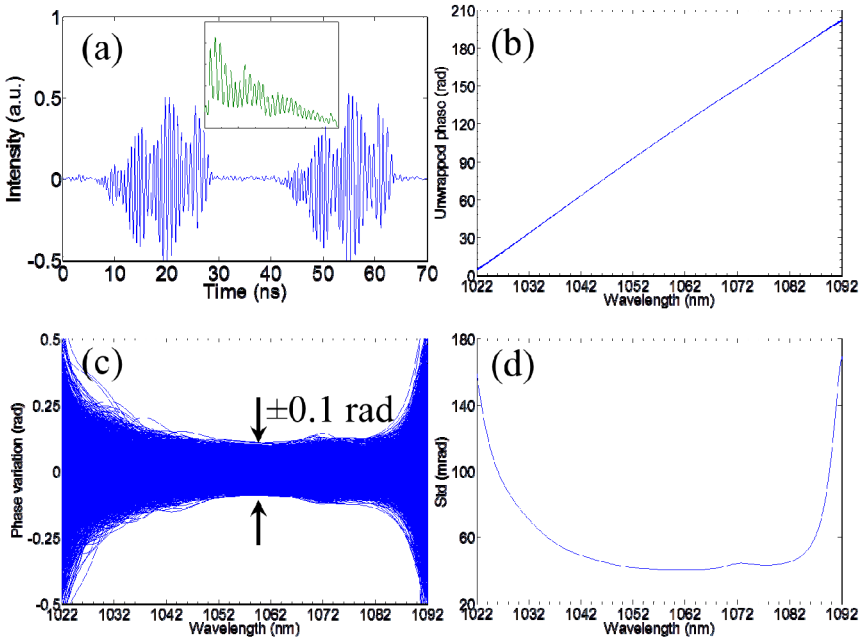

Fig. 5. (a) The train of temporal interferogram with balanced detection. Inset: the corresponding optical spectrum captured by OSA. (b) The unwrapped phases overlapped together. (c) The collection of the phase difference of each sweep referred to their mean. (d) The standard deviation of the phase differences over the sweeping span.

For those phase-sensitive imaging applications, the repeatability of wavelength sweeping from frame to frame, i.e. the wavelength repeatability of the swept source, is very important for signal retrieval [10]. Among those conventional swept sources, an extra k-clock signal is usually required for regular recalibration, owing to their poor wavelength repeatability [11]. BLISS can eliminate the requirement of a dynamic k-clock signal [27]. To illustrate it, we used the pulse output directly from the cavity without time-stretch in fs regime as the trigger of the real-time oscilloscope to observe the temporal self-interferogram, which was generated by the interference between the front and back surfaces of a glass slide. As shown in Fig. 5(a), the temporal interferogram was clean and consistent from sweep to sweep, with balanced detection in real time. The averaged optical spectrum of the interferogram was also captured by a conventional optical spectrum analyzer (OSA), as shown in the inset of Fig. 5(a). To give a quantitative analysis of the phase stability, we recorded a long train of real-time temporal interferogram. Specifically, 5000 consecutive temporal spectra were used to calculate the wavelength repeatability of BLISS by extracting the phases over the interferogram, equivalent to the auto-correlation of the wavelength-swept source [10]. The unwrapped phase of each interferogram was calculated and collected as shown in Fig. 5(b). As can be observed, the interferogram phases of 5000 consecutive sweeps are tightly overlapped with each other. The phase difference of each sweep referred to their mean was calculated and collected in Fig. 5(c), while their standard deviation as the function of the scanning wavelength is shown in Fig. 5(d). As shown in Fig. 5(c), even at a 28.3-MHz sweep rate, BLISS exhibits a phase variation of ± 0.1 rad/sweep over a span of 200 rad, i.e. 0.05%. The superior phase/wavelength repeatability can also be confirmed by Fig. 5(d), giving a standard deviation of ~40 mrad.

#245496 Received 6 Jul 2015; revised 18 Aug 2015; accepted 31 Aug 2015; published 8 Sep 2015

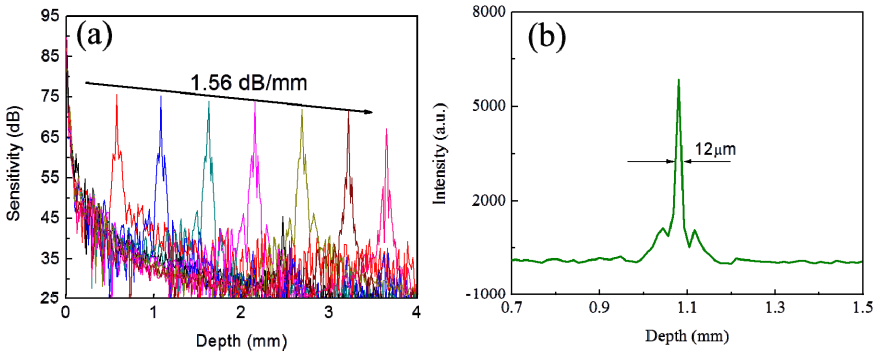

Fig. 6. (a) The sensitivity roll-off characteristic of the 1.0-μm BLISS. (b) The measured axial resolution.

The all-optical swept source was finally launched into the iTS microscope for high-speed single-shot imaging, as shown in Fig. 1. In brief, the wavelength-swept laser beam was first split into two paths through a 50/50 optical coupler, served as the reference arm and sample arm, respectively, in a Michelson interferometer configuration. The one-dimensional spectral shower was generated by a diffraction grating (Richardson Gratings Ltd.), with a groove density of 1200 lines/mm. It was illuminated onto the sample through an objective lens (OL, NA = 0.66), and was then reflected back by using another OL and a mirror at the end, which performs a double-pass transmission configuration. The spatial coordinates are encoded into the optical spectrum of the spectral shower. As BLISS pulse has already been wavelength-swept, the spatial information of the sample can be detected with a single-pixel detection scheme in time domain [15]. To study the sensitivity of the imaging system, we employed the standard characterization method for those Fourier-domain OCT systems [37]. In brief, a Michelson interferometer was implemented by replacing the grating of Fig. 1 with a mirror while another mirror was served as the sample. It equally split the laser beam into the sample and reference arms. Then the interference signal was collected with varying optical path difference between sample and reference arms. Finally, the sensitivity was calculated by measuring the SNR of the signal peak after discrete Fourier transform (DFT) and adding the loss from a neutral density filter, as shown in Fig. 6. It illustrates the sensitivity roll-off characteristic of the BLISS-based interferometric imaging system, and indicates a sensitivity roll-off of 1.56 dB per mm. It should be noted that the sensitivity roll-off dropped more significantly beyond ~3.5 mm because of the frequency response characteristic of the photodetector used in this work. Although the theoretical axial resolution can be as good as 7.8 μm, the non-Gaussian-shape spectrum profile has induced side lobes in the axial signal and thus reduced the axial resolution, i.e. 12 μm as shown in Fig. 6(b). The 6-dB coherence length is 3.8 mm, and it should be pointed out that, a longer coherence length can be obtained by simply increasing the total dispersion amount, i.e. GVD [21,27,38].

#245496 Received 6 Jul 2015; revised 18 Aug 2015; accepted 31 Aug 2015; published 8 Sep 2015

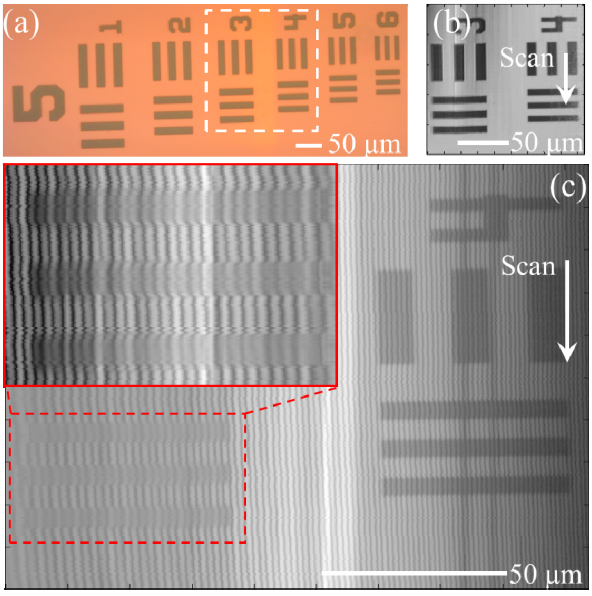

Fig. 7. (a) The light microscope image of the resolution target. (b)-(c) The iTS images with blocked and unblocked reference arm, respectively. Noted, a different scale is used for (c) to clearly illustrate those dense interference fringes.

Figure 7 illustrates the iTS image of a resolution target, Thorlabs USAF-1951, with a chromium coating thickness of 0.120 μm. The imaged area was element 3 and 4 of group 5, with a linewidth of ~10 μm, as shown in Fig. 7(a) captured by a commercial light microscope with a slow imaging speed, i.e. ~60 fps. Benefiting from our flexible configuration, iTS system can also provide an intensity image by simply blocking the reference arm, as shown in Fig. 7(b), where the spectral shower was along the horizontal direction while the single-shot scanning was along the vertical direction. As can be observed, iTS system exhibits comparable intensity imaging quality even at a 28-MHz line-scan rate and a lateral resolution of 1.2 μm, which was measured with the method presented in our prior work [38]. By unblocking the reference arm, the interferometric imaging of the resolution target was captured (see the interferometric image illustrated in Fig. 7(c)). In addition to the intensity image with blocked reference arm, the interferometric image reveals the spatial fringe variation that well corresponds to the resolution target topographic profile, even with sub-μm coating thickness, as observed from the inset of Fig. 7(c). This is made possible with the stable performance brought by BLISS and is important for accurate quantitative phase evaluation at high speed [33,39]. To further exemplify the interferometric imaging performance of the high-speed 1.0-μm BLISS for biological specimen, we performed iTS imaging of a fixed mouse lung tissue section with hematoxylin and eosin (H&E) staining on a fixed glass slide. Figure 8(a) shows the corresponding image of the lung tissue captured by the conventional light microscope, while Fig. 8(b) illustrates the intensity iTS image at a 28-MHz line-scan rate. Again, the high-speed single-shot image shows quality similar to that obtained from the slow light microscope. The interferometric pattern of the lung tissue was imaged by unblocking the reference arm, as shown in Fig. 8(c), where the fringe variation owing to the optical phase shift across the transparent tissue is clearly revealed. Then, the fringe pattern was used to retrieve the quantitative phase profile of the specimen, as shown in Fig. 8(d), through phase image reconstruction [33]. As a consequence, both morphology and phase profile of the biological sample can be captured in a 28-MHz line-scan rate from this BLISS-based iTS microscope, meanwhile the extracted phase profile can be used for further quantitative analysis of the specimen characteristics, e.g. sphericity, mass, etc.

#245496 Received 6 Jul 2015; revised 18 Aug 2015; accepted 31 Aug 2015; published 8 Sep 2015

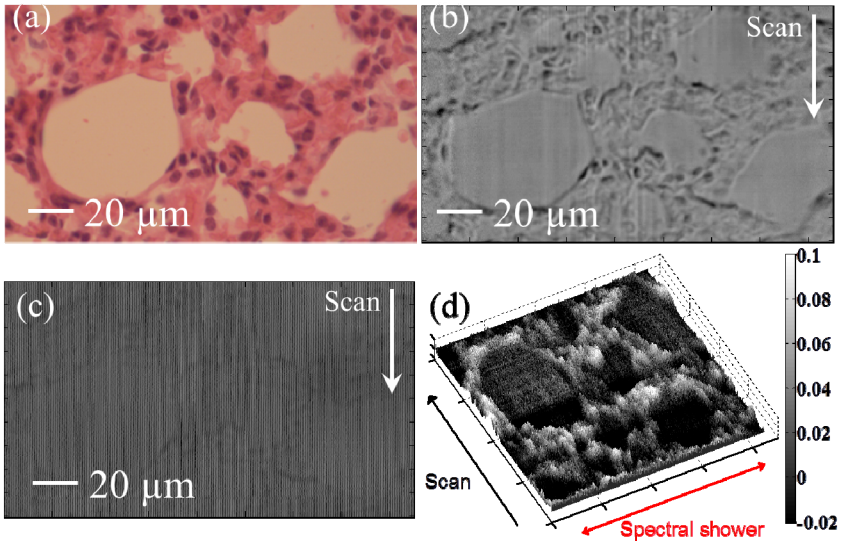

Fig. 8. (a) The light microscope image of the lung tissue. (b)-(c) The iTS images with blocked and unblocked reference arm, respectively. (d) The quantitative phase profile of the mouse lung tissue, retrieved from (c). The color bar represents the phase in radians.

4. Conclusion

In conclusion, we have demonstrated a stable 1.0-μm inertia-free swept source at an ultrafast sweep rate — ~1.76 nm/ns (given a bandwidth of 63 nm at 28 MHz), especially for the ultrafast interferometric imaging. It enables a tunable wavelength sweep range, from ~10 nm to ~63 nm. Both intensity stability and wavelength repeatability have been studied, and a superior performance at such a high sweep rate is identified. As a potential application, it is applied to the phase-sensitive iTS microscopy. Ultrafast interferometric imaging with a resolution of 1.2 μm is obtained at line-scan rate of 28 MHz. It should be emphasized that, the application of this broadband fiber-based inertia-free laser at 1.0 μm can be applied to those established imaging modalities, such as OCT, of which a spatial resolution better than 12 μm (experimentally, while theoretically 7.8 μm) can be achieved.

Acknowledgments

This work was partially supported by grant from the Research Grants Council of the Hong Kong Special Administrative Region, China (Project No. HKU 17205215, HKU 17208414, HKU 7172/12E, HKU ITS/189/13, HKU InP/069/14, HKU InP/238/14, HKU 17207714, HKU 717911E, HKU 720112E) and University Development Fund of HKU.

#245496 Received 6 Jul 2015; revised 18 Aug 2015; accepted 31 Aug 2015; published 8 Sep 2015